Wong, Y. T., K. Halupka, T. Kameneva, S. L. Cloherty, D. B. Grayden, A. N. Burkitt, H. Meffin, and M. N. Shivdasani. 2016. Spectral distribution of local field potential responses to electrical stimulation of the retina. *Journal of Neural Engineering*. **13**(3): 036003.

doi: https://doi.org/10.1088/1741-2560/13/3/036003

Spectral Distribution of Local Field Potential Responses to Electrical Stimulation of the Retina

Short Title: LFP responses to electrical stimulation

Yan T. Wong[1,4], Kerry Halupka[1,2,3], Tatiana Kameneva[1], Shaun L. Cloherty[1,4,5], David B. Grayden[1,3,6], Anthony N. Burkitt[1,3], Hamish Meffin[4,5], Mohit N. Shivdasani[3]

[1] Electrical and Electronic Engineering, The University of Melbourne, VIC 3010, Australia.
[2] National ICT Australia, Victoria Research Lab, The University of Melbourne, VIC 3010, Australia.
[3] Bionics Institute, 384-388 Albert St, East Melbourne, VIC 3002, Australia.
[4] National Vision Research Institute, Australian College of Optometry, Carlton, VIC 3053, Australia.
[5] Australian Research Council Centre of Excellence for Integrative Brain Function, Department of Optometry and Vision Sciences, The University of Melbourne, Melbourne, VIC 3010, Australia.
[6] Centre for Neural Engineering, The University of Melbourne, VIC 3010, Australia.

Correspondence should be addressed to:
Yan Tat Wong, PhD
Tel: +61 3 8344 4222
E-mail: wong.y@unimelb.edu.au
Address: Dept. of Electrical & Electronic Engineering
The University of Melbourne
Victoria 3010
Australia

Word counts

Abstract	253
Introduction	741
Methods	1834
Results	2227
Discussion	1573
References	48
Figures	8
Total words	9056

Abstract

Objective: Different frequency bands of the local field potential (LFP) have been shown to reflect neuronal activity occurring at varying cortical scales. As such, recordings of the LFP may offer a novel way to test the efficacy of neural prostheses and allow improvement of stimulation strategies via neural feedback. Here we use LFP measurements from visual cortex to characterize neural responses to electrical stimulation of the retina. We aim to show that the LFP is a viable signal that contains sufficient information to optimize the performance of sensory neural prostheses. *Approach:* Clinically relevant electrode arrays were implanted in the suprachoroidal space of one eye in four felines. LFPs were simultaneously recorded in response to stimulation of individual electrodes using penetrating microelectrode arrays from the visual cortex. The frequency response of each electrode was extracted using multi-taper spectral analysis and the uniqueness of the responses was determined via a linear decoder. *Main Results:* We found that cortical LFPs are reliably modulated by electrical stimulation of the retina and that the responses are spatially localized. We further characterized the spectral distribution of responses, with maximum information being contained in the low and high gamma bands. Finally, we found that LFP responses are unique to a large range of stimulus parameters (~40) with a maximum conveyable information rate of 6.1 bits. *Significance:* These results show that the LFP can be used to validate responses to electrical stimulation of the retina and we provide the first steps towards using these responses to provide more efficacious stimulation strategies.

Keywords: Local field potential, vision prosthesis, retinal prosthesis, decoding

Introduction

In recent years, there have been many advances toward restoring useful visual perception to people suffering from vision loss. Specifically, human trials involving retinal prostheses that target surviving retinal neurons with electrical stimulation have shown that these devices can aid in rudimentary activities ranging from simple light localization to independent navigation and even reading large font (Fujikado et al., 2011; Zrenner et al., 2011; Dorn et al., 2013; Ayton et al., 2014). Success of these trials has led to the first retinal visual prostheses now being commercially available (Ho et al., 2015; Stingl et al., 2015).

While successful human implantations have demonstrated the promise of these devices in providing artificial vision, there are still significant limitations such as low spatial and temporal resolution and challenges in selectively activating specific retinal neurons (Zrenner, 2013). Animal studies provide a complimentary path to test novel stimulation methods that may solve some of these issues (Wong et al., 2009; Dumm et al., 2014). Specifically, studies that allow recording of neural signals in response to electrical stimulation provide an optimal way to test and fine-tune stimulation parameters (Priori et al., 2013; Jepson et al., 2014a, 2014b).

Many studies have focused on measures of spiking activity since it reflects the output of a single neuron or up to tens of neurons. However, the local field potential (LFP) may provide a more suitable signal for the optimization of stimulus parameters. The LFP is defined as the low frequency components (typically < 300 Hz) of neural activity and is thought to be generated by the summation of transmembrane currents (Mitzdorf, 1985). The different frequency components of the LFP are also hypothesized to reflect neuronal processes occurring at different cortical scales (Buzsáki et al., 2012). The LFP is a measure of the population activity across an area of cortex as opposed to the activity of a single neuron and, therefore, is more stable and easier to record (Flint et al., 2012). As a population metric, the LFP also has the advantage of being less biased by the stochastic nature of sampling individual neuron firing rates (Panzeri et al., 2007).

Therefore, the LFP has emerged as an important signal for a variety of different neural prostheses such as brain-machine interfaces (Markowitz et al., 2011; Flint et al., 2013) and deep brain stimulators (Priori et al., 2013). In these examples, the LFP has been used either as a primary signal to control a prosthetic device or as a neural feedback signal to fine-tune stimulation parameters.

However, the recording stability may result in a lower spatial resolution of information conveyed, potentially limiting the LFP's usefulness for neural prostheses that require high spatial resolution. From experiments in the visual system, it has been estimated that measures of the LFP integrate activity across an area of ~250 µm from the tip of a microelectrode (Katzner et al., 2009; Xing et al., 2009). Whether the LFP can provide neural feedback with such resolution for electrical stimulation from a visual prosthesis is unknown (Waldert et al., 2009).

Early studies showed that cortical LFPs could be broadly modulated by electrical stimulation of the retina from epi-retinal and sub-retinal implant placements (Schanze et al., 2002; Eckhorn et al., 2006). Cottaris *et al.* (2009) then showed that the broadband LFP power could be used to decode electrode configurations and stimulus parameters for stimulation of the retina from the epi-retinal space. The LFP decoder was used to characterize the performance of their epi-retinal approach via an information metric, finding a maximum conveyed information rate of ~4.25 bits with 64 different stimulation parameters.

In this work, we comprehensively investigate the frequency and phase responses of the LFP to electrical stimulation of the retina from the suprachoroidal space (Sakaguchi et al., 2004; Wong et al., 2009; Cicione et al., 2014) and use the LFP to compare the maximum information deliverable by this device to that of other retinal approaches. This is the first study to analyze multi-site LFP responses to suprachoroidal stimulation; our results show that the LFP is highly informative about the stimulation parameters. The study shows also that suprachoroidal stimulation generates discriminable cortical LFP responses with a close correspondence from stimulus to response. Furthermore, all experiments that we present utilize electrode arrays similar to those used in recent human trials by Bionic Vision Australia (Ayton et al., 2014; Shivdasani et al., 2014), allowing results to be directly relatable to clinical practice.

Materials and methods

Anesthesia and surgery

Data were collected from four normally sighted adult cats (n=4) implanted with a stimulating electrode array in the suprachoroidal space of a single eye and a recording array in the contralateral visual cortex. All procedures were approved by the Bionics Institute Animal Ethics Committee (formerly the Royal Victorian Eye and Ear Hospital Animal Ethics Committee; Projects 12/255AB and 14/304AB). Each animal was initially anaesthetized with ketamine (20 mg/kg, intramuscular (i.m.)) and xylazine (2 mg/kg subcutaneous (s.c.)) and maintained with a continuous intravenous infusion of sodium pentobarbitone (60 mg/kg/hr). Animals were given daily doses of dexamethasone (0.1 mg/kg i.m.) to reduce brain swelling and antibiotics (clavulox, 10 mg/kg s.c.). Pupils were dilated with a topical application of phenylephrine hydrochloride (2.5%) and tropicamide (1%). A continuous infusion of fluid (Hartmann's solution 1.5 mg/ml/hr) was provided and the respiration rate, end-tidal CO_2, and core body temperate were monitored.

To implant the stimulating electrode array, a full-thickness incision was made through the sclera approximately 5 mm behind the corneal limbus and then a 'pocket' was opened within the suprachoroidal space (Saunders et al., 2014). The arrays were implanted ~15 mm into the pocket so that the electrode contacts were situated in the area centralis. The stimulating electrode arrays contained 21 circular platinum electrodes each with an exposed diameter of 600 µm and were organized in a staggered 3 x 7 grid, with two large (2 mm diameter) return electrodes on the proximal end of the array. The center-to-center spacing between electrodes was 1 mm, which equates to a visual angle of ~4º (Hubel and Wiesel, 1959).

For the recording electrode, a craniotomy was performed over the visual cortex (Tusa et al., 1978) in the contralateral hemisphere to the eye with the stimulating electrode and the dura mater was removed. To record neural activity, penetrating microelectrode arrays (60 channels, 6 x 10 arrangement, 1 mm length, 400 µm spacing, Blackrock Micro., USA) were implanted into the visual cortex. The location of implantation of the cortical array was optimized with respect to the location of the stimulating array determined using evoked potential recordings from the cortical surface in response to retinal stimulation

as described in previous studies (Cicione et al., 2014; Dumm et al., 2014). All cortical recordings were referenced to a platinum wire inserted into the temporal muscle.

Electrical stimulation and neural signal recording methods

In all animals, cortical responses to single electrode retinal stimulation were recorded. The stimuli used were single cathodic-leading biphasic current pulses (500 µs per phase, 25 µs interphase gap) on one electrode at a time. In all animals, currents from 0 to 1.5 mA (corresponding to a maximum safe charge density of less than 300µC/cm^2 per phase) were tested in 100 µA increments; in one animal (a55) further tests were done in 50 µA increments. Each stimulation amplitude was repeated ten times in random order at a repetition rate of 1 Hz. A subset of electrodes that were not utilized to deliver charge to the retina due to time constraints or technical reasons were removed from further analysis.

Neural signals were recorded at a sampling rate of 30 kHz (Blackrock Micro., USA). To obtain the LFP, the broadband signal (0.1 Hz – 7.5 kHz) was low-pass filtered at 400 Hz using a multitaper-spectral technique (Thomson, 1982; Mitra and Pesaran, 1999) (multitaper projection filter settings; [Time duration = 25 ms, Frequency bandwidth = 400 Hz, Center frequency = 0 Hz]). The LFP signal was then down-sampled to 2.5 kHz. The spectrum of the LFP for time steps pre- and post-stimulation were then estimated (MATLAB, MathWorks, USA) with a temporal resolution of 0.8 ms, a frequency resolution of 2.5 Hz, and a 16 ms Hamming window. The time-frequency spectrograms presented were normalized to the average power in each recording channel 0 - 50 ms before the stimulus onset. For all figures, the mean and standard error of the mean has been shown unless otherwise stated.

To test for significant changes in LFP power in the time-frequency spectrograms, a permutation test was performed comparing the power in each frequency and time period after the stimulus to the power in the 50 ms preceding the stimulus. A minimum of 10,000 permutations were performed for each test. To correct for multiple comparisons, cluster correction to a significance level of $p < 0.05$ was applied to the statistical tests (Maris et al., 2007). To classify electrodes as exhibiting significant evoked responses, a single Wilcoxon Rank sum test was performed ($p < 0.05$) at ~110 Hz, 13 ms after the stimulus pulse onset (chosen due to the peak in the responses). To analyze how significant responses

spread across the cortex with changing stimulus parameters, we calculated a normalized weighted distance measure,

$$D = \frac{\sum_i r_i d_i}{\sum_i r_i},$$

where r_i is the magnitude of the response on a given cortical electrode, i, and d_i is the cortical distance in mm from electrode i to the electrode on the array with the maximal response.

To estimate how the spatial spread of responses across the cortical electrodes could correspond to perceived visual experiences, the width of the cortical response was calculated and a cortical magnification factor of 0.3-0.5 mm/deg was used. This was derived from the cortical recording locations' anatomical maps (Tusa et al., 1978) and prior studies (Walter et al., 2005). Significant changes in the phase of the LFP were then tested using a permutation test (10,000 permutations) against the phase in the 50 ms period before the stimulus. Bonferroni correction was used to control for multiple comparisons to a level of $p < 0.05$. Finally, the effect of stimulating electrode location on cortical response shift was examined by first finding the cortical recording channel with the largest response to stimulation at 300 µA. Then, the relative Euclidean distance between the electrodes with maximal response was calculated as a function of the distance between the stimulating electrodes used to generate the response. Here we assumed a cortical magnification factor of 0.3 mm/deg regardless of eccentricity (Tusa et al., 1978).

Decoding stimulus features and characterizing with an information metric

To test the uniqueness of the evoked responses, the LFP was decoded to predict the electrical stimulation parameters used to generate the responses (stimulating electrode identity and current level). The decoding algorithm was comprised of three stages: preprocessing, extraction of features, and classification (Markowitz et al., 2011). In the preprocessing stage, for each trial and each recording channel, a time window of LFP data was extracted and transformed into the frequency domain (described above). The resulting frequency domain data across all the recording channels was collapsed to form a single vector of a length determined by the number of recording channels (60) multiplied by the number of frequency bins (160 for all LFP frequency bands, 1-400 Hz). Essentially, frequency bands and recording channel identities were removed and treated independently with one vector representing the response to

each stimulation trial and time window. This was repeated for each trial and for time windows before and after the stimulus.

Decoding was performed at individual time points that varied from 20 ms before stimulation to 100 ms after. The decoding performance of four different spectral bands (1-30 Hz, 40-100 Hz, 101-300 Hz, and 1-400 Hz) corresponding roughly to beta, low-gamma, high-gamma, and all frequency bands was also tested. Frequency steps were identical for all groupings. To do this, the signal in each spectral band was estimated before performing the previously described preprocessing methods.

Next, to reduce the dimensionality of these vectors, an orthogonal transformation (Principle Component Analysis, PCA) was used to generate a set of uncorrelated features. The 150 features that captured the most variance of the original space were used by the decoder to predict the stimulation parameters. This number was chosen through an iterative process, where the number of features was increased and the decoding performance of a random sample of data examined. With increasing features, the decoding performance plateaued and a point beyond the plateau was chosen. This was done through a linear discriminant analysis, which effectively clustered the feature responses to different stimulation parameters (electrode number and stimulation level) (Duda et al., 2012). As an example, when decoding responses from two different stimulus parameters (or classes; $U_{trial} \in \{0, 1\}$), the analysis fitted a linear, discriminant function, $f(x)$, that best separated the transformed neural activity in response to the two classes. The discriminant function is given by

$$f(x) = w^T x + a$$

$$w = \mathrm{C}^{-1}(\mu_2 - \mu_1)$$

$$a = -w^T \mu$$

where x is the feature vector of the PCA transformed, frequency domain neural responses. The w parameters for the above equation were fit using training data that included an equal number of responses from both classes, with μ_1 and μ_2 representing the means of each class, μ the mean of both classes, and C the pooled covariance of both classes.

To decode class labels for a separate test set, $f(x)$ is calculated for each trial of data in the set and assigned to class 0 if $f(x) < 0$ or to, class 1 if $f(x) \geq 0$. To extend this to decoding more than two

stimulus parameters, a one-vs-all classification approach was taken, where a binary decoder was created for all class pairs. Class labels were then assigned by

$$k = \underset{i}{\operatorname{argmax}} \sum_{j} f_{ij}(x)$$

where $f_{ij}(x)$ denotes the decoder for classes i and j, and k the classified class label. The decoding estimates from the above method were bootstrapped using a leave-one-out cross validation method.

Finally, to test differences in the information contained in the magnitude and phase of the LFP, the decoding was performed by calculating and including either the phase (represented as a number in $[0, 2\pi)$), magnitude, or both phase and magnitude in the preprocessing stage. For this comparison, all other stages of decoding remained the same. In this manuscript, the mean correct performance of decoding averaged across all decoded parameters is shown, as well as confusion matrices that detail how each stimulation parameter was predicted. Confusion matrices are plotted for data taken from the first positive peak after the stimulation pulse.

To characterize the performance of suprachoroidal stimulation in generating uniquely discriminable responses and to compare this to previously published results from other stimulation locations such as the epi-retinal approach, a mutual information metric described by Cottaris *et al.* (2009) was calculated. Specifically, we calculated the mutual information, $I(\tilde{S}; S)$, between the decoded stimulation parameters, $\tilde{S}$, and the actual stimulation parameters, S. This is given by

$$I(\tilde{S}; S) = \sum_{u=1}^{N} \sum_{v=1}^{N} P_{\tilde{S}S}(u, v) log \frac{P_{\tilde{S}S}(u, v)}{P_{\tilde{S}}(u) P_S(v)}$$

where $P_{\tilde{S}}(u)$ and $P_S(v)$ are the marginal probability distributions with

$$P_{\tilde{S}}(u) = \sum_{v=1}^{N} P_{\tilde{S}S}(u, v)$$

and

$$P_S(v) = \sum_{u=1}^{N} P_{\tilde{S}S}(u, v) = \frac{1}{N}$$

as each stimulation parameter was presented an equal number of times. Here, u represents the individual stimulus parameters presented (from 1 to N), and v represents the decoded stimulus parameter identities

from the classifier described in the earlier section. Information metrics were also corrected for bias using a Miller-Madow correction where the bias, B, is given by

$$\mathrm{B} = \frac{\hat{\mathrm{m}} - 1}{2\mathrm{n}},$$

where $\hat{\mathrm{m}}$ is the number of bins with non-zero probabilities and n is the number of samples (Miller, 1955; Panzeri et al., 2007). To measure how well each individual stimulus parameter was decoded from the rest, a sensitivity index, d', was calculated for each stimulus parameter (Cottaris and Elfar, 2009):

$$d' = Z(hit\ rate) - Z(false\ alarm\ rate)$$

where Z represents the z-score of each probability of detection. The "hit rate" is the probability that a given stimulus parameter (e.g. current level 1 from electrode 1) is correctly identified (as current level 1 from electrode 1), whereas the "false alarm rate" is the probability of other stimulus parameters (stimuli 2 to N) being incorrectly classified as stimulus 1.

Finally, to calculate how mutual information varied with different set sizes (the number of available stimulation parameters), d' was used to iteratively remove the worst decoded stimulus parameter. In this analysis, all stimulus parameters were decoded at the first iteration. For every subsequent iteration, the stimulus parameter with the lowest d', which reflected the least well decoded parameter, was removed from the set and the decoder was re-run. This was performed until only a single stimulus parameter was left. To test the robustness of this method, the same analysis was repeated but, instead of removing the stimulus parameter with the lowest d', a stimulus parameter in the lowest ten was randomly chosen and removed from subsequent iterations. For the time stepped decoding analysis, three currents were decoded on each electrode (100, 500, and 1000 µA) chosen from thresholds and dynamic ranges previously reported (Cicione et al., 2014; Dumm et al., 2014). For the mutual information analysis, currents ranging over 0 - 1.5 mA in 100 µA steps for three animals and in 50 µA steps for one animal were decoded.

Results

Local field potentials are modulated by electrical stimulation

There was a robust and immediate neural response to electrical stimulation of the retina delivered from the suprachoroidal space. The broadband signals showed an initial peak within 10 ms of the stimulus and a secondary peak after 20 ms. The amplitude of the initial peak increased in magnitude as the current level was increased. The broadband response recorded on a single recording channel following electrical stimulation of a single stimulating electrode in the suprachoroidal space is shown in **Figure 1a**. The peaked response and ordering seen in the broadband signal remained after filtering to obtain the LFP (**Fig. 1b**). The large stimulus artifact, which is prominent in the broadband response (peak at 0 ms), was suppressed in the LFP averages, as would be expected for a biphasic pulse with phase durations of 500 µs.

Time-frequency decompositions of the LFP signals were calculated from these responses to allow the information carried in each frequency band and the time evolution of this information to be compared across recording channels and stimulating electrodes. The resulting spectrograms (**Fig. 1c**) showed that a significant double-peaked response occurred in the range 100-200 Hz (black lines show regions with significant changes from baseline period power, $p < 0.05$ cluster-correct Permutation test). With increasing current levels, the power within this band increased.

To examine whether these effects existed across the population of responses, all combinations of recording channels and stimulating electrodes were tested for a significant response at four different current levels (0, 200, 500, and 700 µA). **Figure 2a** illustrates the population response using the same conventions as in **Figure 1c**. In total, 4380 stimulating/recording pairs were tested, with the number of significant pairings stated on the top right of each panel. A significant increase in power between 100-200 Hz was again prominent in the population average with multiple peaks visible. With increasing current levels, power in this band increased, the number of recording channels showing a significant response increased, and a third peak in the response between 40-50 ms became significant (stimulus current > 500 µA).

In addition to the magnitude of the LFP response, the instantaneous phase was also significantly modulated by electrical stimulation. **Figure 2b** shows the corresponding population average phase

changes at ~110 Hz to the four different levels of stimulation. Significant changes in the phase from baseline are indicated by asterisks above each plot. These results show that the LFP was modulated reliably and broadly by electrical stimulation in the suprachoroidal space.

LFP responses are spatially localized

The previous analyses examined responses on individual electrodes; however, an important aspect for visual prostheses is the relationship between stimulus parameters and the spatial extent of the evoked response. As expected for increasing stimulating current levels, the spread of the response increased across the recording channels. An example of this is illustrated in **Figure 3**, where the response across all the cortical recording channels (60) to two different current levels delivered from a single stimulating electrode is shown. The response to 100 μA stimulation (**Fig. 3a**) was more focused spatially than the response to 250 μA stimulation (**Fig. 3b**). The response was also lower in magnitude on individual electrodes that did respond. For these examples, the response at the peak of the spectrum 240 Hz, ~15 ms post stimulus is plotted in **Figures 3c** and **3d**.

To quantify these trends across electrodes and animals, the number of recording channels that responded significantly at different time points, different frequencies, and to different current levels delivered from the stimulating electrodes was characterized. As expected, the number of significant recording channels increased as a function of stimulus current with an average of 4.4 ± 1.4 electrodes (mean ± s.e.) showing a significant response at 200 μA (corresponding to a visual angle of 1.6 º -2.7º), eventually plateauing at ~28 electrodes at 1.2 mA (**Fig. 3e**). Further increases in current did not lead to a further increase in the number of significantly activated electrodes (1.2 mA: 28.4 ± 2.4 electrodes, 1.5 mA: 28.3 ± 2.4, $p = 0.96$; Rank sum test). Tests for significance were performed at 240 Hz, ~15 ms after the stimulus onset at the peak of the average response.

When examining the spread of activity as a function of time (**Fig. 3f**), two clear peaks were present with a third smaller but significant peak at 40 ms ($p = 10\ e^{-5}$; Signed-rank test). For **Figure 3f**, tests for significance were performed at 240 Hz for a 1 mA stimulus. Finally, when looking at how activity spread as a function of the frequency band of interest, the number of significant channels increases to a peak at 300 Hz (**Fig. 3g**). Tests for significance were performed ~15 ms after a 1 mA stimulus

corresponding to the first peak shown in **Figure 3f**. When the extent of the spread of activity was analyzed using a normalized weighted distance metric, D, the same trend in results as above emerged (**Fig. 3h-j**). The only major difference occurred 40 ms post stimulus with the spatial spread of the response increasing markedly even though the number of significant channels only changed by a few electrodes (**Fig. 3f** vs. **3i**).

Finally, we analyzed how the locations of the cortical responses shifted depending on the locations of the stimulating electrodes. Figure 4 presents the average shift in the location of the maximum response as a function of the shift in stimulus location for pairs of retinal electrodes (n=505). The location of cortical responses shifted when the retinal stimulus location shifted; however, the degree of displacement was much less than expected from the known retinotopic mapping. This shift also plateaus with larger displacements of the stimulus location. Regardless, these results show that the LFP can be a reliable signal to test for the spread of activity in the visual cortex and that the spread and location of activity is dependent on the amplitude of stimulation, the time period after the stimulus, and the frequency band that is tested.

LFP responses are unique to different stimuli

While reliably eliciting percepts is important for a visual prosthesis, the efficacy of the implant is highly dependent on the ability to generate a large set of distinguishable percepts. Neural responses to electrical stimulation that are distinguishable from each other would indicate that the resultant percepts may be unique and differentiated from each other. As such, a linear classifier was implemented to decode stimulus parameters from the LFP signals to test the ability to discriminate between the elicited neural responses. For this analysis, the LFP cortical responses from all recording channels to three stimulus amplitudes (100, 500, and 1000 μA, chosen to correspond to three clinically relevant current levels, (Shivdasani et al., 2014)) delivered via each of 19 stimulating electrodes was decoded (two electrodes were removed due to insufficient responses). The decoding was performed using all LFP frequencies (1-400 Hz) initially on a single time window of data. This window was then advanced one time-step at a time and the analysis repeated.

The LFP was found to be highly informative, with a peak decoder performance of ~75% in a single subject (**Fig. 5a**). This suggests that the LFP response is stable across trials and informative of the majority of stimulus configurations (i.e. 19x3 = 57 stimulating electrodes and current level combinations). However, it is evident from **Figure 5a** that the decoder performance exhibited a strong temporal effect. Decoding performance shared similar features to the multipeaked responses seen in the spectrograms, with two large prominent peaks. However, this feature was not present in the population decoding performance (**Fig. 5b**), which exhibited a single peak in the decoding performance.

The decoding performance of individual stimulus parameters was further broken up to show where the classification confusions lie. Data from the first peak in **Figure 5a** were used to generate the confusion matrix shown in **Figure 5c**. The axes are grouped and sorted according to stimulating electrode so that the first three small squares represented current levels 100, 500, and 1000 μA, respectively, on the stimulating electrode 1, the next three squares represented the same currents on stimulating electrode 2, and so on. From this, the majority of stimulus parameters were decoded with a success rate greater than 85% and most confusions occur for the lower current stimuli (100 μA). This may be due to the current levels on these electrodes being subthreshold to generate a response and hence the resulting neural activity for currents below this level being identical.

To better analyze how the LFP differed in response to the stimulation parameters, the full set of stimuli (31 current levels, 19 electrodes) were decoded and confusion matrices were generated that collapsed stimulus labels across either the stimulating electrode (**Fig. 5d**) or the current level (**Fig. 5e**). This analysis revealed that the stimulating electrode identity was encoded in the LFP with high fidelity and that all could be decoded significantly above chance ($p < 0.05$; Binomial test). Interestingly, when comparing how well current levels could be decoded from the neural responses, a pattern emerged where currents above a certain level were more confused (bottom right of **Fig. 5e**) compared to the middle and low ranges of currents. This result is consistent with the plateauing of the spatial spread of response previously presented in **Figure 3e** and **3h**.

LFP information is frequency dependent

Since previous results showed that the spread of activity across the cortical recording array was frequency dependent (**Fig. 3g**), the decoding performances of band-limited neural signals were next compared. Three frequency bands of interest were chosen: beta (1-30 Hz), low gamma (40-100 Hz), and high gamma (101-300 Hz). **Figures 6a** and **b** present the results from a single animal and for the population average, respectively. Beta band activity was consistently the least informative frequency band, with low and high gamma bands having equal decoding performance during the first peak. In the example shown in **Figure 6a**, information in the low gamma band was more informative than the high gamma band in the second peak ($p = 0.001$; Rank sum test at ~29 ms after stimulus), with this effect being smaller but still significant across the population average ($p = 0.011$; Rank sum test).

In order to test whether the temporal information in the LFP was consistent, or whether the first and second peaks in the response conveyed different information about the stimulus, the decoder was re-run using all LFP frequencies (1-400 Hz) in the data from either the first peak alone or from both the first and second peaks. Information contained in the peaks were found to be redundant with the decoding performance of both decoders is statistically indistinguishable (1^{st} peak: 57.4±4.2%, 1^{st} and 2^{nd} peaks: 56.3±4.5%, $p = 0.74$; Rank sum test).

LFP phase provides an alternate source of information

The phase of the LFP was shown to be significantly modulated (**Fig. 2c**) by electrical stimulation, but it is unknown whether these changes are informative about the stimulation parameters. To test this, the phase response alone was used to decode the stimulation parameters. This was done with all the frequencies of the LFP (1-400 Hz) and in the three bands previously identified. The phase of the LFP was found to be broadly informative (**Fig. 7a and b**) with the beta band phases again exhibiting the lowest decoding performance similar to the results found when decoding with magnitude. Interestingly, contrary to what we found when using the magnitude alone, decoding performance of the high gamma phases was better than the low gamma phases for the period between 10-15 ms after stimulus onset ($p < 10\ e^{-9}$; Rank sum test). Decoding of all frequency bands was also lower for the phases compared to the performance when decoding with magnitude.

Finally, both signals (amplitude and phase) were used simultaneously to decode the stimulus parameters to examine whether the information in the phase was independent of the amplitude of the LFP. The information in the combined LFP phase and amplitude was redundant with no significant differences (all points $p > 0.05$; Rank sum test) in the combined decoding performance of the phase and magnitude decoder and the magnitude-alone decoder sessions (**Fig. 7c** and **d vs Fig. 6a** and **b**).

Calculating the maximum information conveyed by suprachoroidal stimulation

In order to compare the results of suprachoroidal stimulation to other previously published stimulation approaches, the decoding performance of each session was converted into a standard information metric. This metric was calculated for varying stimulus set sizes. For each session, all stimulus parameter combinations (electrode number and stimulus amplitude, 31 current levels in subject a55, and 16 current levels for all other subjects) were decoded from the magnitude of the LFP, the least informative response was removed (see Methods for more details), and the new set of stimulus parameters were decoded. This was repeated until only one stimulus parameter remained.

Figures 8a and **b** present the mutual information conveyed by the suprachoroidal prostheses (black lines) with the theoretical maximum information shown in red. For this data, the mean and standard deviation across the animals is shown. For the single subject example (**Fig. 8a**), there were approximately 50 highly informative stimulus parameters after which the information content conveyed by more stimulus parameters increased slowly. When all 589 stimulus parameters were included from this experiment, the maximum information delivered was 6.08 bits. To ensure that the method of removing the least informative session was accurate, a randomized removal method was also tested with the information conveyed in these sessions being only slightly less, but not significantly lower (all points $p > 0.05$ Rank sum test), than that with the optimal method (**Fig. 8a**). A smaller set of informative stimulus parameters (~40) was also found in the population average analysis (**Fig 8b**). At a set size of 221 stimulus parameters, there was a maximum information of 5.4 ± 0.47 bits (mean ± std). For smaller set sizes of 64 stimulus parameters, the total information was 5.14 ± 0.6 bits. These analyses were performed at the time point of maximum decoding performance.

The mutual information metric was also used to compare the differences in information being conveyed in each frequency band. **Figures 8c** and **d** present the single animal and population results, respectively. As previously shown, the high and low gamma band contained statistically identical ($p > 0.05$; Rank sum test) information, whereas the beta band was the least informative. This effect remained for decreasing set sizes of the stimulation parameters.

Discussion

The main aim of this work was to examine the properties of the LFP response that can be used to test the effectiveness of neural prostheses. We found that the LFP was highly informative about the stimulus parameters used to evoke responses and that responses were distinguishable and reproducible to a wide range of stimulus parameters (~40). We also found that the electrically evoked LFP response was multi-peaked, with the first peak the most informative in the low and high gamma frequency bands and that the magnitude of the response was the most informative. When examining the evoked responses with an information metric, we also found that suprachoroidal stimulation was able to provide similar if not more distinguishable responses than certain epi-retinal devices (6.1 bits from a total stimulus set size of 589). These results provide strong evidence that time-frequency decompositions of the LFP can be used to provide feedback in designing new stimulus paradigms and that the stimulation from the suprachoroidal space is effective in generating distinguishable cortical responses.

Neural feedback and the LFP

In a clinical setting, recording of the LFP during electrical stimulation would allow dynamic adjustment of stimulation parameters based on inferring the perceived phosphenes. Ideally, these stimulation parameters would be continuously altered until the responses more closely mimic those elicited by natural light stimulation. Adjustment of stimulation parameters (fitting) has been shown to be a necessary strategy for maximizing auditory perception in cochlear implants (Wilson and Dorman, 2008). In cochlear implants, stimulation parameters are fine-tuned for each electrode in response to subject feedback. For a device such as a visual prosthesis, due to a need for substantially larger numbers of stimulating electrodes, tuning of parameters based on overt subject responses will not be clinically feasible. Using a stable, reliable, and easily recorded signal such as the LFP may provide the feedback necessary to adjust stimulation parameters dynamically and on-line (Flint et al., 2012, 2013), circumventing this issue.

There still remains significant difficulty in defining an objective function that will maximize the usability of a vision prosthesis for a patient. In particular, there is no clear way to optimize cortical responses to the many complex natural scenes that are experienced daily (Kayser et al., 2003; Weliky et al., 2003). However, a simple objective function that aims to reduce the cortical spread of responses may

provide significant improvements in vision to patients by generating more punctate phosphenes (Wong et al., 2009).

Another drawback of using a neural signal to provide feedback is, of course, the necessity to implant additional electrodes in the patient. For this reason, the LFP is a particularly attractive choice compared to the use of spiking activity because it can be recorded with less invasive electrodes, such as micro-ECoG or EEG, whereas spiking activity must be recorded with a penetrating electrode and would be less stable over the long periods of time that would be required of a prosthesis. Work in the field of brain-machine interfaces in animals has shown that ECoG recordings can offer decoding performance as good as penetrative LFP recordings (Chao et al., 2010), with some success in translating this to humans (Wolpaw et al., 2002; Leuthardt et al., 2004). However, there have also been results to the contrary where from a simple information viewpoint, penetrating the cortex significantly increases decoding performance (Markowitz et al., 2011). This decrease in available information may reduce the clinical viability of using dynamic feedback to improve the efficacy of visual prostheses.

Cortical evoked responses

The responses recorded from the visual cortex, evoked by suprachoroidal stimulation in this study were similar in shape and timing to those previously reported for epi-retinal and sub-retinal stimulation (Eckhorn et al., 2006; Cottaris and Elfar, 2009; Wong et al., 2009). Consistent with these studies, the peak-to-peak magnitude of the broadband response and the spread of the response across the visual cortex increased with increasing stimulus charge delivered. The extent of this spatial spread of activity was found to plateau, which indicates a maximum level of cortical activation. Interestingly, at the lower end of the stimulus levels, we found that a 200 µA stimulus on average activated four cortical recording channels (**Fig. 3e**). We estimate that this corresponds to an evoked response spanning a visual angle of 1.6º-2.7º. This would be similar to phosphene sizes generated in human trials for suprachoroidal stimulation. Patients have reported experiencing phosphenes similar in size to a ‘dime’ or ‘quarter’ (1.7º-2.2º) at an arm’s length (Fujikado et al., 2007). This is, however, larger than the size of phosphenes reported for epi-retinal and sub-retinal stimulation, which typically range from 0.1º-2º (Humayun et al., 2003; Wilke et al., 2011; Zrenner et al., 2011). The most likely explanation for the increased phosphene

sizes is the current spread resulting from increased distance of the stimulating electrodes from the retinal ganglion cells and the need to stimulate through the choroid.

We also find that the shift in the location of the cortical response is less than expected from the known retinotopic mapping. This may be due to two different reasons. The first is the limited cortical coverage provided by the recording array and the relatively large coverage of the stimulating array. With a width of 4 mm, the recording array is unable to record from all corresponding locations of the retina being stimulated. If this were the case, responses to stimulation of distant, more peripheral locations of the retina would result in measured cortical responses that were centered off the array, on the edge of the array, or deep within the cortical sulci. This is the result that we see (**Fig. 4**), with the displacement of the cortical response plateauing. This would also be consistent with the variable decoding results across electrodes (**Fig. 5c**), with electrodes with poor performance, particularly those that were located more peripherally, perhaps generating responses not centered or as well covered by the recording electrode. The second possibility is that stimulation of the retina is not occurring directly under the electrode and is instead being shunted across the retinal tissue. If this is the case, all electrodes should be affected equally; however, our results show a clear plateauing only for distant locations. Further experiments with greater coverage of the cortex with either more arrays or higher coverage surface electrodes would be required to answer this question.

Frequency dependence of responses

The spatial spread of the LFP response was heavily dependent on the frequency band analyzed. We found that increasing charge injection strongly modulated the activity in the 100-200 Hz (high gamma) frequency band (**Fig. 3g**). There is growing evidence that the LFP may reflect neuronal processes occurring at varying cortical scales. Specifically, it has been hypothesized that different frequency bands of the LFP reflect specific neuronal processes (Siegel et al., 2012). Relevant to the work in this study, the low frequency beta band activity (1-20 Hz) is posited to reflect distributed processing that occurs across large networks of neurons (Fries, 2005; Donner and Siegel, 2011). This is in contrast to low gamma (30-100 Hz) and high gamma (100-200 Hz) bands, which reflect local computations and processing

(Schomburg et al., 2012; Buzsáki and Schomburg, 2015), with the high gamma band activity being more closely related to single unit spiking (Ray and Maunsell, 2011).

Therefore, we posit that the electrical stimulation generates localized responses in the activity of primary visual cortex. However, we find that the spread of activity across the cortex is greatest in the high gamma band, and perhaps due to this spreading of activity, the information about the stimulus parameters is significantly greater in the low gamma band during the second peak of the response (**Figs. 6 a** and **b**). While this effect is small, it is nonetheless significant and may indicate a different mechanism in the activity present in the second peak.

Finally, to examine the LFP responses comprehensively, we also analyzed the information conveyed in the phase of the LFP (**Figs. 7a** and **b**). While the phase was informative, it was significantly less so than the magnitude of the LFP and did not contain any new information as revealed by the combined phase-magnitude decoding analysis. The phase of the LFP has been previously reported to increase the information conveyed with spiking information in the visual system (Gray et al., 1989; Vinck et al., 2010). Future work to investigating the link between activity in these frequency bands and perceived phosphenes may allow for targeted activation of the LFP in specific frequency bands that is coherent with spiking activity (Kayser et al., 2009).

Time dependent information changes

The latency of the first peak of the responses (10-15 ms, **Fig. 1a**) to electrical stimulation showed a similar timing to that reported by other groups (epi-retinal: 10-20 ms (Eckhorn et al., 2006), suprachoroidal: 10-16 ms (Nakauchi et al., 2005; Wong et al., 2009)). This latency is faster than that reported for visual stimulation (> 20ms), which suggests that the photoreceptors have been bypassed and the ganglion cells in the retina were directly activated. In these recordings, we also saw a significant second peak with a latency of 20-30 ms. This secondary peak may arise from secondary indirect activation of the photoreceptors or other retinal neurons, activity mediated by bipolar neurons, or more complex cortico-cortico interactions. From the decoding analysis, we found that the information contained in the second peak was significantly less than that in the first peak and that there was little new information in the second peak (**Fig. 5**). Furthermore, information in the second peak was strongest in the

low gamma band, which is less a reflection of spiking activity than the high gamma band (**Fig. 6b**). This further alludes to the possibility that the second peak in the LFP activity arose from cortico-cortico interactions as opposed to secondary activation from the retina.

Information metric comparators

The information metric allowed the results from this study to be compared to other anatomical locations for a retinal prosthesis. We found that the performance of suprachoroidal stimulation in providing distinguishable cortical responses was greater than the 25 channel epi-retinal device reported by Cottaris and Elfar (2009). They reported an information rate of ~4.25 bits with 64 stimulus parameters whereas we found an average information rate of 5.1 bits for the same number of stimulus parameters (**Fig. 8b**). We also reported a maximum information rate of 6.1 bits for the full stimulus set size (**Fig. 8a**).

By analyzing the confusion matrices for this decoding analysis, we also showed, as expected, that low current stimuli (close to threshold) and stimuli above 1.2 mA did not generate distinguishable responses (**Fig. 3e**). For low current stimuli, we posit that this is due to sub-threshold responses, where no significant change in the recorded waveforms occurs when compared to pre-stimulus periods; high current stimuli would have resulted in consistent saturated responses, leading to our algorithm being unable to decode the correct stimulation parameters.

The greater ability to generate distinguishable responses in this study compared to that reported by Cottaris and Elfar (2009) may be due to a larger stimulus set being tested as well as a larger separation between stimulating electrodes (0.68º for the epi-retinal electrodes vs 4º for electrodes used in these experiments). However, the information metric does highlight the advantages of the suprachoroidal approach in targeting a wide visual field allowing for more unique, easily distinguished responses (~40).

While these analyses do not answer whether the visual system is actually taking advantage of the features used in the decoders, the information metric allows benchmark comparison of the evoked neural responses across experimental paradigms. The analyses, specifically the decoding results, also indicate that a large set of different cortical responses are being evoked through suprachoroidal stimulation and future work may help close the gap between the number of distinguishable cortical responses that can be evoked and spatially distinguishable phoshenes reported by human patients.

References

Ayton LN et al. (2014) First-in-Human Trial of a Novel Suprachoroidal Retinal Prosthesis. PLoS One 9:e115239.

Buzsáki G, Anastassiou CA, Koch C (2012) The origin of extracellular fields and currents--EEG, ECoG, LFP and spikes. Nat Rev Neurosci 13:407–420.

Buzsáki G, Schomburg EW (2015) What does gamma coherence tell us about inter-regional neural communication? Nat Neurosci 18:484–489.

Chao ZC, Nagasaka Y, Fujii N (2010) Long-term asynchronous decoding of arm motion using electrocorticographic signals in monkeys. Front Neuroeng 3:3.

Cicione R, Fallon JB, Rathbone GD, Williams CE, Shivdasani MN (2014) Spatiotemporal interactions in the visual cortex following paired electrical stimulation of the retina. Invest Ophthalmol Vis Sci 55:7726–7738.

Cottaris NP, Elfar SD (2009) Assessing the efficacy of visual prostheses by decoding ms-LFPs: application to retinal implants. J Neural Eng 6:026007.

Donner TH, Siegel M (2011) A framework for local cortical oscillation patterns. Trends Cogn Sci 15:191–199.

Dorn JD, Ahuja AK, Caspi A, da Cruz L, Dagnelie G, Sahel J-A, Greenberg RJ, McMahon MJ (2013) The Detection of Motion by Blind Subjects With the Epiretinal 60-Electrode (Argus II) Retinal Prosthesis. JAMA Ophthalmol 131:183–189.

Duda RO, Hart PE, Stork DG (2012) Pattern Classification. John Wiley & Sons.

Dumm G, Fallon JB, Williams CE, Shivdasani MN (2014) Virtual electrodes by current steering in retinal prostheses. Invest Ophthalmol Vis Sci 55:8077–8085.

Eckhorn R, Wilms M, Schanze T, Eger M, Hesse L, Eysel UT, Kisvárday ZF, Zrenner E, Gekeler F, Schwahn H, Shinoda K, Sachs H, Walter P (2006) Visual resolution with retinal implants estimated from recordings in cat visual cortex. Vision Res 46:2675–2690.

Flint RD, Lindberg EW, Jordan LR, Miller LE, Slutzky MW (2012) Accurate decoding of reaching movements from field potentials in the absence of spikes. J Neural Eng 9:046006.

Flint RD, Wright ZA, Scheid MR, Slutzky MW (2013) Long term, stable brain machine interface performance using local field potentials and multiunit spikes. J Neural Eng 10:056005.

Fries P (2005) A mechanism for cognitive dynamics: neuronal communication through neuronal coherence. Trends Cogn Sci 9:474–480.

Fujikado T, Kamei M, Sakaguchi H, Kanda H, Morimoto T, Ikuno Y, Nishida K, Kishima H, Maruo T, Konoma K, Ozawa M, Nishida K (2011) Testing of semichronically implanted retinal prosthesis by suprachoroidal-transretinal stimulation in patients with retinitis pigmentosa. Invest Ophthalmol Vis Sci 52:4726–4733.

Fujikado T, Morimoto T, Kanda H, Kusaka S, Nakauchi K, Ozawa M, Matsushita K, Sakaguchi H, Ikuno Y, Kamei M, Tano Y (2007) Evaluation of phosphenes elicited by extraocular stimulation in normals and by suprachoroidal-transretinal stimulation in patients with retinitis pigmentosa. Graefe's Arch Clin Exp Ophthalmol 245:1411–1419.

Gray CM, König P, Engel AK, Singer W (1989) Oscillatory responses in cat visual cortex exhibit inter-columnar synchronization which reflects global stimulus properties. Nature 338:334–337.

Ho AC et al. (2015) Long-Term Results from an Epiretinal Prosthesis to Restore Sight to the Blind. Ophthalmology 122:1547–1554.

Hubel DH, Wiesel TN (1959) Receptive fields of single neurones in the cat's striate cortex. J Physiol 148:574–591.

Humayun MS, Weiland JD, Fujii GY, Greenberg R, Williamson R, Little J, Mech B, Cimmarusti V, Van Boemel G, Dagnelie G, de Juan E (2003) Visual perception in a blind subject with a chronic microelectronic retinal prosthesis. Vision Res 43:2573–2581.

Jepson LH, Hottowy P, Mathieson K, Gunning DE, Dąbrowski W, Litke AM, Chichilnisky EJ (2014a) Spatially patterned electrical stimulation to enhance resolution of retinal prostheses. J Neurosci 34:4871–4881.

Jepson LH, Hottowy P, Weiner GA, Dabrowski W, Litke AM, Chichilnisky EJ (2014b) High-fidelity reproduction of spatiotemporal visual signals for retinal prosthesis. Neuron 83:87–92.

Katzner S, Nauhaus I, Benucci A, Bonin V, Ringach DL, Carandini M (2009) Local origin of field potentials in visual cortex. Neuron 61:35–41.

Kayser C, Montemurro MA, Logothetis NK, Panzeri S (2009) Spike-phase coding boosts and stabilizes information carried by spatial and temporal spike patterns. Neuron 61:597–608.

Kayser C, Salazar RF, Konig P (2003) Responses to natural scenes in cat V1. J Neurophysiol 90:1910–1920.

Leuthardt EC, Schalk G, Wolpaw JR, Ojemann JG, Moran DW (2004) A brain-computer interface using electrocorticographic signals in humans. J Neural Eng 1:63–71.

Maris E, Schoffelen J-M, Fries P (2007) Nonparametric statistical testing of coherence differences. J Neurosci Methods 163:161–175.

Markowitz DA, Wong YT, Gray CM, Pesaran B (2011) Optimizing the Decoding of Movement Goals from Local Field Potentials in Macaque Cortex. J Neurosci 31:18412–18422.

Miller G (1955) Note on the bias of information estimates. Inf theory Psychol Probl Methods II-B:95–100.

Mitra PP, Pesaran B (1999) Analysis of dynamic brain imaging data. Biophys J 76:691–708.

Mitzdorf U (1985) Current source-density method and application in cat cerebral cortex: investigation of evoked potentials and EEG phenomena. Phys Rev 65:37–100.

Nakauchi K, Fujikado T, Kanda H, Morimoto T, Choi JS, Ikuno Y, Sakaguchi H, Kamei M, Ohji M, Yagi T, Nishimura S, Sawai H, Fukuda Y, Tano Y (2005) Transretinal electrical stimulation by an intrascleral multichannel electrode array in rabbit eyes. Graefe's Arch Cinical Exp Ophthalmol 243:169–174.

Panzeri S, Senatore R, Montemurro MA, Petersen RS (2007) Correcting for the sampling bias problem in spike train information measures. J Neurophysiol 98:1064–1072.

Priori A, Foffani G, Rossi L, Marceglia S (2013) Adaptive deep brain stimulation (aDBS) controlled by local field potential oscillations. Exp Neurol 245:77–86.

Ray S, Maunsell JHR (2011) Different origins of gamma rhythm and high-gamma activity in macaque visual cortex. PLoS Biol 9:e1000610.

Sakaguchi H, Fujikado T, Fang X, Kanda H, Osanai M, Nakauchi K, Ikuno Y, Kamei M, Yagi T, Nishimura S, Ohji M, Yagi T, Tano Y (2004) Transretinal electrical stimulation with a suprachoroidal multichannel electrode in rabbit eyes. Jpn J Ophthalmol 48:256–261.

Saunders AL, Williams CE, Heriot W, Briggs R, Yeoh J, Nayagam DAX, McCombe M, Villalobos J, Burns O, Luu CD, Ayton LN, McPhedran M, Opie NL, McGowan C, Shepherd RK, Guymer R, Allen PJ (2014) Development of a surgical procedure for implantation of a prototype suprachoroidal retinal prosthesis. Clin Experiment Ophthalmol 42:665–674.

Schanze T, Wilms M, Eger M, Hesse L, Eckhorn R (2002) Activation zones in cat visual cortex evoked by electrical retina stimulation. Graefe's Arch Clin Exp Ophthalmol 240:947–954.

Schomburg EW, Anastassiou CA, Buzsáki G, Koch C (2012) The spiking component of oscillatory extracellular potentials in the rat hippocampus. J Neurosci 32:11798–11811.

Shivdasani MN, Sinclair NC, Dimitrov PN, Varsamidis M, Ayton LN, Luu CD, Perera T, McDermott HJ, Blamey PJ (2014) Factors affecting perceptual thresholds in a suprachoroidal retinal prosthesis. Invest Ophthalmol Vis Sci 55:6467–6481.

Siegel M, Donner TH, Engel AK (2012) Spectral fingerprints of large-scale neuronal interactions. Nat Rev Neurosci 13:121–134.

Stingl K et al. (2015) Subretinal Visual Implant Alpha IMS - Clinical trial interim report. Vision Res 111:149–160.

Thomson DJ (1982) Spectrum estimation and harmonic analysis. Proc IEEE 70:1055–1096.

Tusa RJ, Palmer LA, Rosenquist AC (1978) The retinotopic organization of area 17 (striate cortex) in the cat. J Comp Neurol 177:213–235.

Vinck M, Lima B, Womelsdorf T, Oostenveld R, Singer W, Neuenschwander S, Fries P (2010) Gamma-phase shifting in awake monkey visual cortex. J Neurosci 30:1250–1257.

Waldert S, Pistohl T, Braun C, Ball T, Aertsen A, Mehring C (2009) A review on directional information in neural signals for brain-machine interfaces. J Physiol Paris 103:244–254.

Walter P, Kisvárday ZF, Görtz M, Alteheld N, Rossler G, Stieglitz T, Eysel UT (2005) Cortical activation via an implanted wireless retinal prosthesis. Invest Ophthalmol Vis Sci 46:1780–1785.

Weliky M, Fiser J, Hunt RH, Wagner DN (2003) Coding of Natural Scenes in Primary Visual Cortex. Neuron 37:703–718.

Wilke R, Gabel V-P, Sachs H, Bartz Schmidt K-U, Gekeler F, Besch D, Szurman P, Stett A, Wilhelm B, Peters T, Harscher A, Greppmaier U, Kibbel S, Benav H, Bruckmann A, Stingl K, Kusnyerik A, Zrenner E (2011) Spatial resolution and perception of patterns mediated by a subretinal 16-electrode array in patients blinded by hereditary retinal dystrophies. Invest Ophthalmol Vis Sci 52:5995–6003.

Wilson BS, Dorman MF (2008) Cochlear implants: a remarkable past and a brilliant future. Hear Res 242:3–21.

Wolpaw JR, Birbaumer N, McFarland DJ, Pfurtscheller G, Vaughan TM (2002) Brain–computer interfaces for communication and control. Clin Neurophysiol 113:767–791.

Wong YT, Chen SC, Seo JM, Morley JW, Lovell NH, Suaning GJ (2009) Focal activation of the feline retina via a suprachoroidal electrode array. Vis Res 49:825–833.

Xing D, Yeh C-I, Shapley RM (2009) Spatial spread of the local field potential and its laminar variation in visual cortex. J Neurosci 29:11540–11549.

Zrenner E (2013) Fighting blindness with microelectronics. Sci Transl Med 5:210ps16.

Zrenner E, Bartz-Schmidt KU, Benav H, Besch D, Bruckmann A, Gabel V-P, Gekeler F, Greppmaier U, Harscher A, Kibbel S, Koch J, Kusnyerik A, Peters T, Stingl K, Sachs H, Stett A, Szurman P, Wilhelm B, Wilke R (2011) Subretinal electronic chips allow blind patients to read letters and combine them to words. Proc Biol Sci / R Soc 278:1489–1497.

Acknowledgements

The authors wish to thank Felix Aplin, Patrick Atkinson, Rosemary Cicione, Sam John, and Ronald Leung for assistance with data collection, Michelle McPhedran and Alexia Saunders for technical assistance, Penelope Allen and Jonathan Yeoh who performed all surgeries, and Owen Burns, Helen Feng, and Vanessa Maxim for electrode array fabrication. We also wish to thank Rob Shepherd, Chris Williams and James Fallon for overall guidance and advice during the *in vivo* experiments. This research was supported by the Australian Research Council's *Discovery Projects* funding scheme (DP140104533) and through its Special Research Initiative in Bionic Vision Science and Technology awarded to Bionic Vision Australia. The research was also supported by the Bertalli Family Foundation through the Bionics Institute. The Bionics Institute acknowledges the support received from the Victorian Government through its Operational Infrastructure Program. This research was supported by a Victorian Life Sciences Computation Initiative (VLSCI) grant number [VR0138] on its Peak Computing Facility at the University of Melbourne, an initiative of the Victorian Government, Australia.

Figure Legends

Figure 1. Example of an averaged **(a)** broadband (0.01 – 7.5 kHz) and **(b)** local field potential (0.1 - 400 Hz) response to suprachoroidal electrical stimulation of the retina at different current levels. Each stimulus was delivered with a biphasic pulse with a phase duration of 500 µs. Responses increased in amplitude with increasing current levels. The stimulus artifact contamination (at 0 ms) in the broadband average was not dominant after filtering to generate the local field potential average. **(c)** Time-frequency spectrograms of the local field potential responses shown in panel (b). Spectrograms were normalized to the baseline power 50 ms pre-stimulus and significant changes in power from baseline are indicated with black lines.

Figure 2. (a) Population average responses (magnitude of the spectrum of the LFP) across all animals to four current levels. Only recording channels that exhibited a significant response from baseline were averaged. The number of significant recording channel-stimulating electrode combinations for each stimulation level is shown in the top right hand corner of each spectrogram. A significant change in power of the LFP can be seen shortly after the stimulus onset (highlighted with a black line $p < 0.05$ cluster-corrected Rank sum test). At 0 µA current, channels with a non-significant response are shown. **(b)** The population average of the instantaneous phase (at ~110 Hz) of the LFP in response to the same stimulation parameters. Significant changes in the phase from baseline are indicated with stars ($p < 0.05$, Bonferroni corrected permutation test). The mean ± s.t.d. are shown.

Figure 3. (a) Example spectrograms across the 60 recording channels in response to a 100 µA stimulus from one animal. Each individual panel shows the time-frequency response on one recording channel. The panels are spatially arranged in the same organization as the recording array (i.e. 6x10 grid). In this example, a small localized response can be seen in the middle left of the array. **(b)** With increasing current, responses increased in magnitude and spread across the array. **(c,d)** The response across the cortex for the examples presented in **(a)** and **(b).** The magnitude of the response at 240 Hz and ~15 ms post stimulus across the 6x10 array are shown. Data has been interpolated. Superimposed in white, is the idealized approximate response spread for a retinal electrode diameter of 600 µm and a cortical magnification of 0.3 mm/deg. The cortical spread was summarized by **(e)** examining the number of channels that significantly responded to a stimulus as a function of the charge injected, **(f)** the time point at which the significance test was performed, and **(g)** the frequency at which the significance test was performed. The size of the spread of the response was also characterized for **(h)** increasing currents, **(i)** different time points, and **(j)** different frequencies. For **(e)**-**(j)** the mean ± s.e.m. are shown.

Figure 4. The change in the location of the maximal cortical response as a function of the change in the location of the stimulation site on the retina. Cortical distance has been converted to visual angle using a spatial mapping of 0.3 mm/deg. The mean and s.e.m. are shown.

Figure 5. (a) Example from one animal showing the probability of correctly decoding the stimulation parameters (electrode identity and current level) at different time points before and after the stimulus pulse. Shortly after the stimulus was delivered, the decoding performance increased significantly. The mean ± s.e.m. are shown. **(b)** Population average decoding performance. **(c)** A confusion matrix for the example in (a), showing the joint distribution of the predicted and observed stimulation parameters. Gray

lines indicate the groupings of currents delivered from a single stimulating electrode. The 19 gray lines indicate groupings of 3 current levels tested for each prediction. **(d)** A confusion matrix showing the decoding performance for the example in (a) collapsed across electrode identities (decoding electrode identities but not current levels). **(e)** A confusion matrix showing the decoding performance for the example in (a) collapsed across current levels (decoding current levels but not electrode identities).

Figure 6. (a) Frequency-band limited decoding performance of the stimulus parameters for a single animal. The mean ± s.e.m. are shown. **(b)** Population decoding performance for the same band-limited frequency inputs.

Figure 7. Decoding performance of the phase of the LFP as a function of time. **(a)** Example from one animal using data from all frequencies as well as when the data were separated according to the different frequency bands. The mean ± s.e.m. are shown. **(b)** Similar to panel (a), but for the population average data. **(c)** Decoding performance of the combined phase and magnitude of the LFP in one animal, and **(d)** for the population average.

Figure 8. Mutual information as a function of stimulus parameter set size. **(a)** Mutual information (black lines) for a single animal when the “optimal” and “pseudo-random” removal of the least informative stimulus parameters is used. The red lines show the theoretical maximum amount of information that can be conveyed with each stimulus set size. **(b)** Population average mutual information. For (a) and (b), all frequency bands of the LFP were used. Mutual information of the three frequency bands of interest **(c)** for the single animal example **(d)** and for the population average. Mutual information for low gamma and high gamma results are overlapping for panels (c) and (d). The mean ± std are shown.

Figure 1

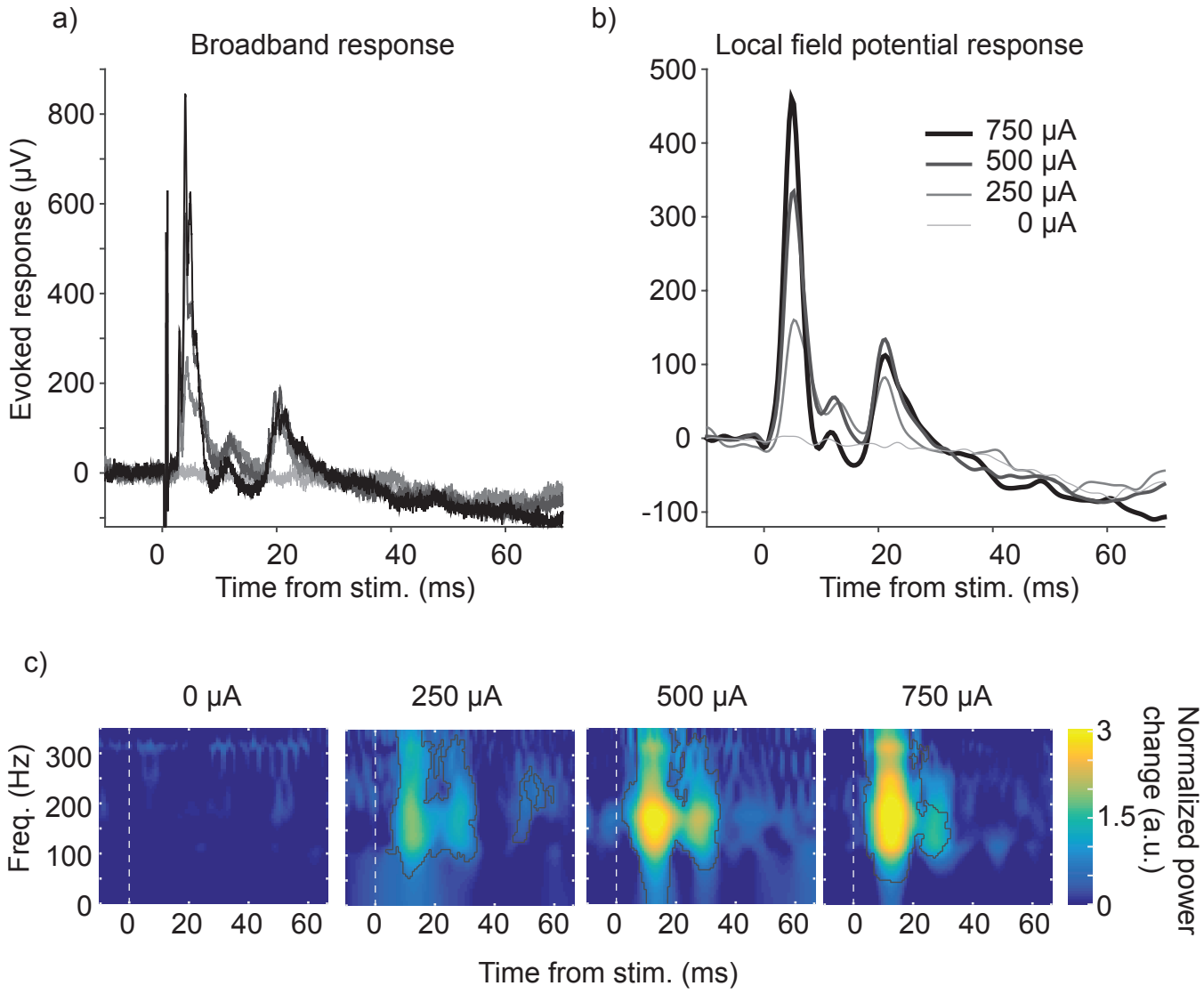
a)
Broadband response
Evoked response (μV)
800
600
400
200
0
0
20
40
60
Time from stim. (ms)
b)
Local field potential response
500
400
300
200
100
0
-100
750 μA
500 μA
250 μA
0 μA
0
20
40
60
Time from stim. (ms)
c)
0 μA
250 μA
500 μA
750 μA
Freq. (Hz)
300
200
100
0
0
20
40
60
3
1.5
0
Normalized power change (a.u.)
Time from stim. (ms)

Figure 2

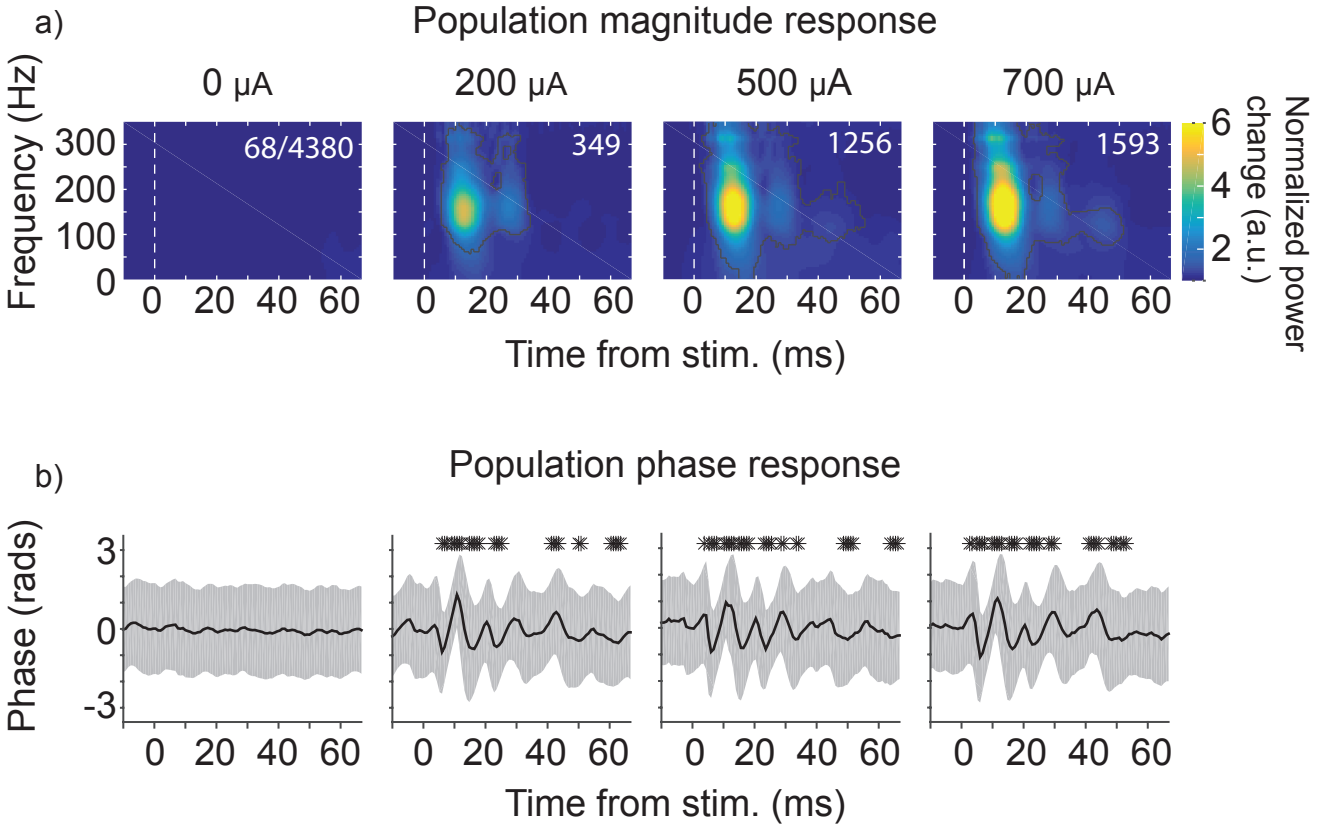
a)
Population magnitude response
0 µA
200 µA
500 µA
700 µA
Frequency (Hz)
300
200
100
0
68/4380
349
1256
1593
0 20 40 60
Time from stim. (ms)
Normalized power change (a.u.)
6
4
2
b)
Population phase response
Phase (rads)
3
0
-3
0 20 40 60
Time from stim. (ms)

Figure 3

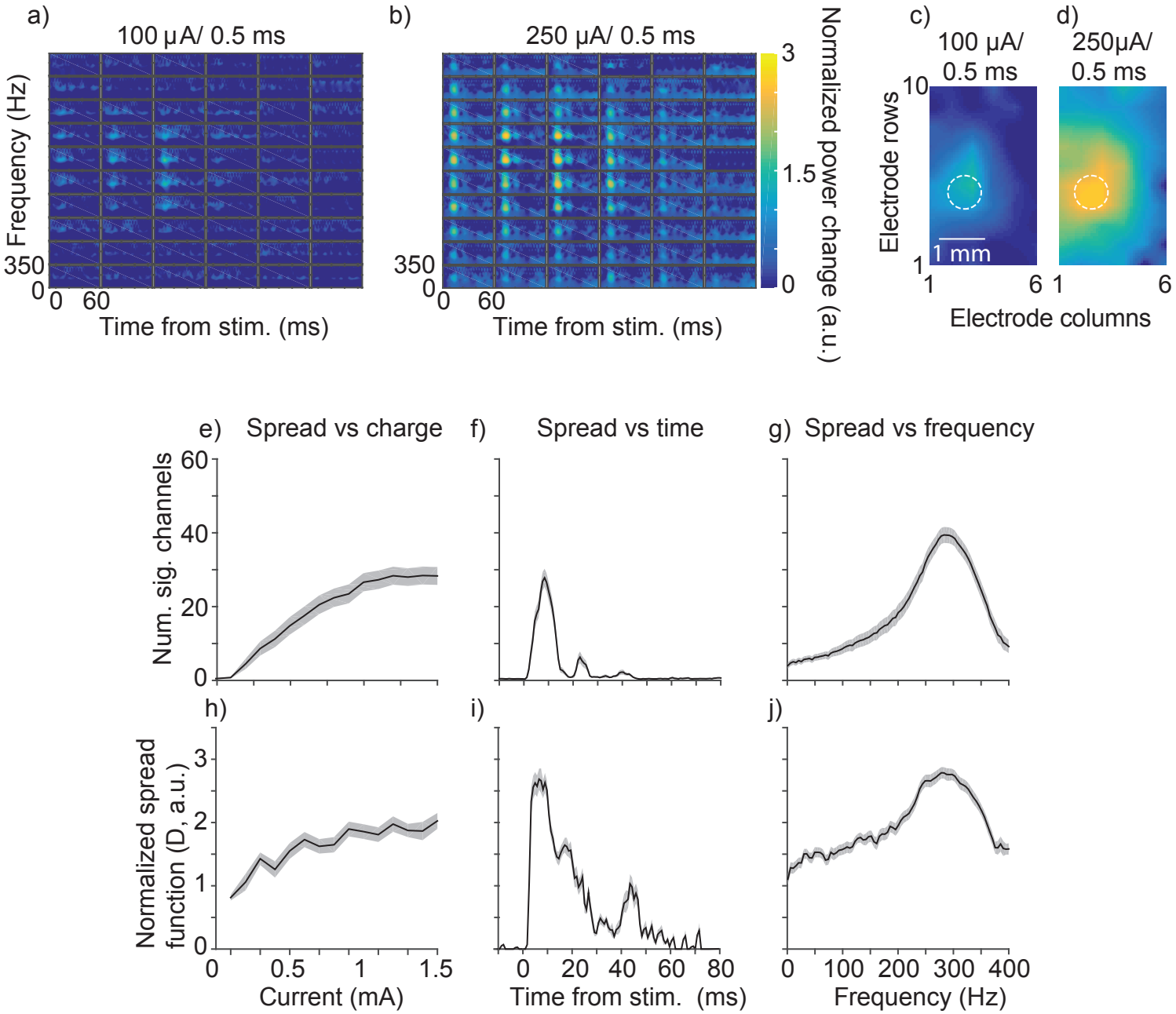
a)
100 µA/ 0.5 ms
Frequency (Hz)
350
0
0 60
Time from stim. (ms)
b)
250 µA/ 0.5 ms
350
0
0 60
Time from stim. (ms)
3
1.5
0
Normalized power change (a.u.)
c)
100 µA/
0.5 ms
d)
250µA/
0.5 ms
Electrode rows
10
1
1 mm
1 6
1 6
Electrode columns
e) Spread vs charge
f) Spread vs time
g) Spread vs frequency
Num. sig. channels
60
40
20
0
h)
i)
j)
Normalized spread
function (D, a.u.)
3
2
1
0
0 0.5 1 1.5
Current (mA)
0 20 40 60 80
Time from stim. (ms)
0 100 200 300 400
Frequency (Hz)

Figure 4

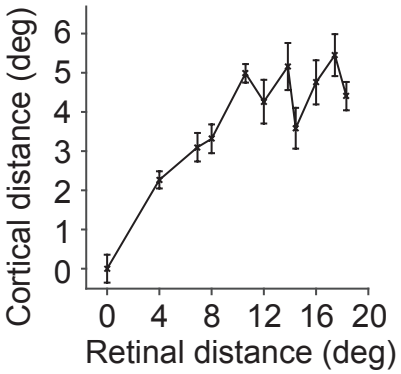
Cortical distance (deg)
0
1
2
3
4
5
6
0
4
8
12
16
20
Retinal distance (deg)

Figure 5

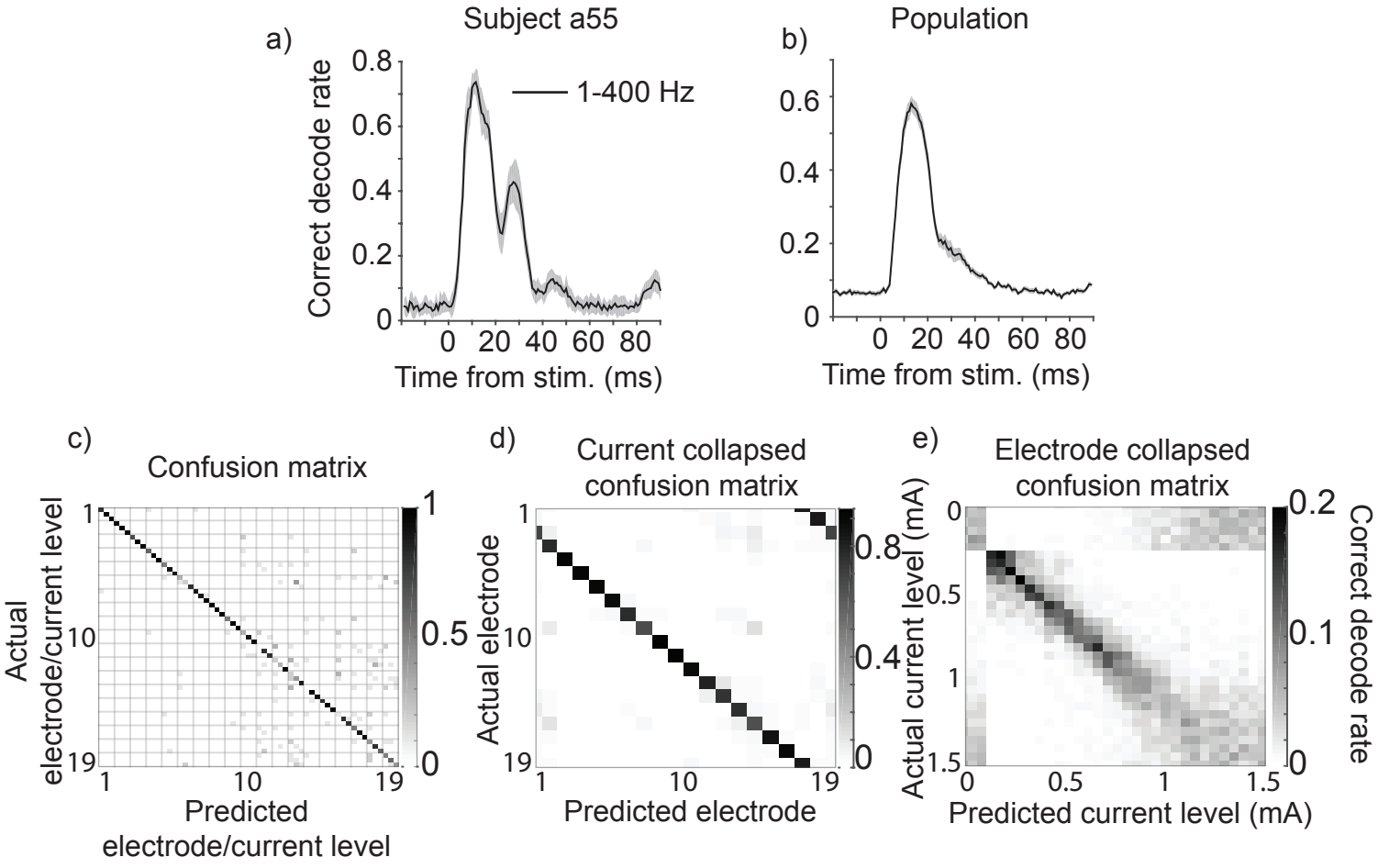
a)
Subject a55
Correct decode rate
1-400 Hz
Time from stim. (ms)
b)
Population
Time from stim. (ms)
c)
Confusion matrix
Actual electrode/current level
Predicted electrode/current level
d)
Current collapsed confusion matrix
Actual electrode
Predicted electrode
e)
Electrode collapsed confusion matrix
Actual current level (mA)
Predicted current level (mA)
Correct decode rate

Figure 6

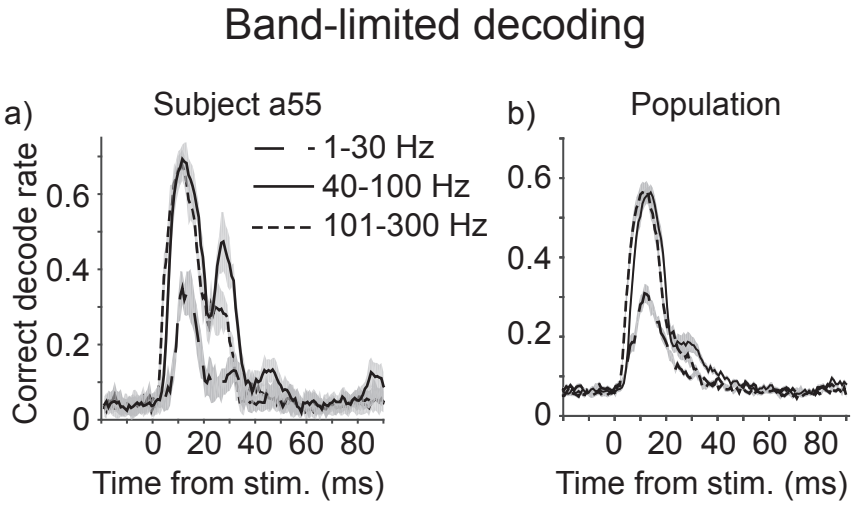
Band-limited decoding
a)
Subject a55
1-30 Hz
40-100 Hz
101-300 Hz
Correct decode rate
0
0.2
0.4
0.6
0 20 40 60 80
Time from stim. (ms)
b)
Population
0
0.2
0.4
0.6
0 20 40 60 80
Time from stim. (ms)

Figure 7

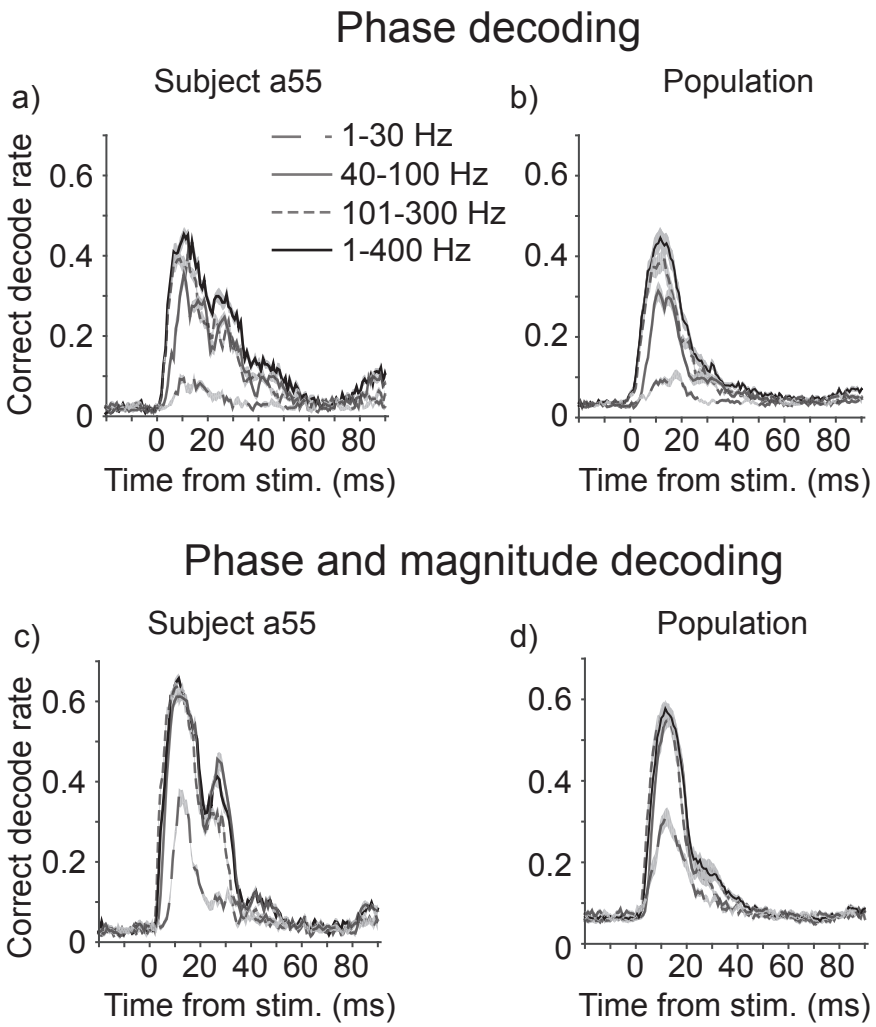
Phase decoding
a)
Subject a55
1-30 Hz
40-100 Hz
101-300 Hz
1-400 Hz
Correct decode rate
0.6
0.4
0.2
0
0 20 40 60 80
Time from stim. (ms)
b)
Population
0.6
0.4
0.2
0
0 20 40 60 80
Time from stim. (ms)
Phase and magnitude decoding
c)
Subject a55
Correct decode rate
0.6
0.4
0.2
0
0 20 40 60 80
Time from stim. (ms)
d)
Population
0.6
0.4
0.2
0
0 20 40 60 80
Time from stim. (ms)

Figure 8

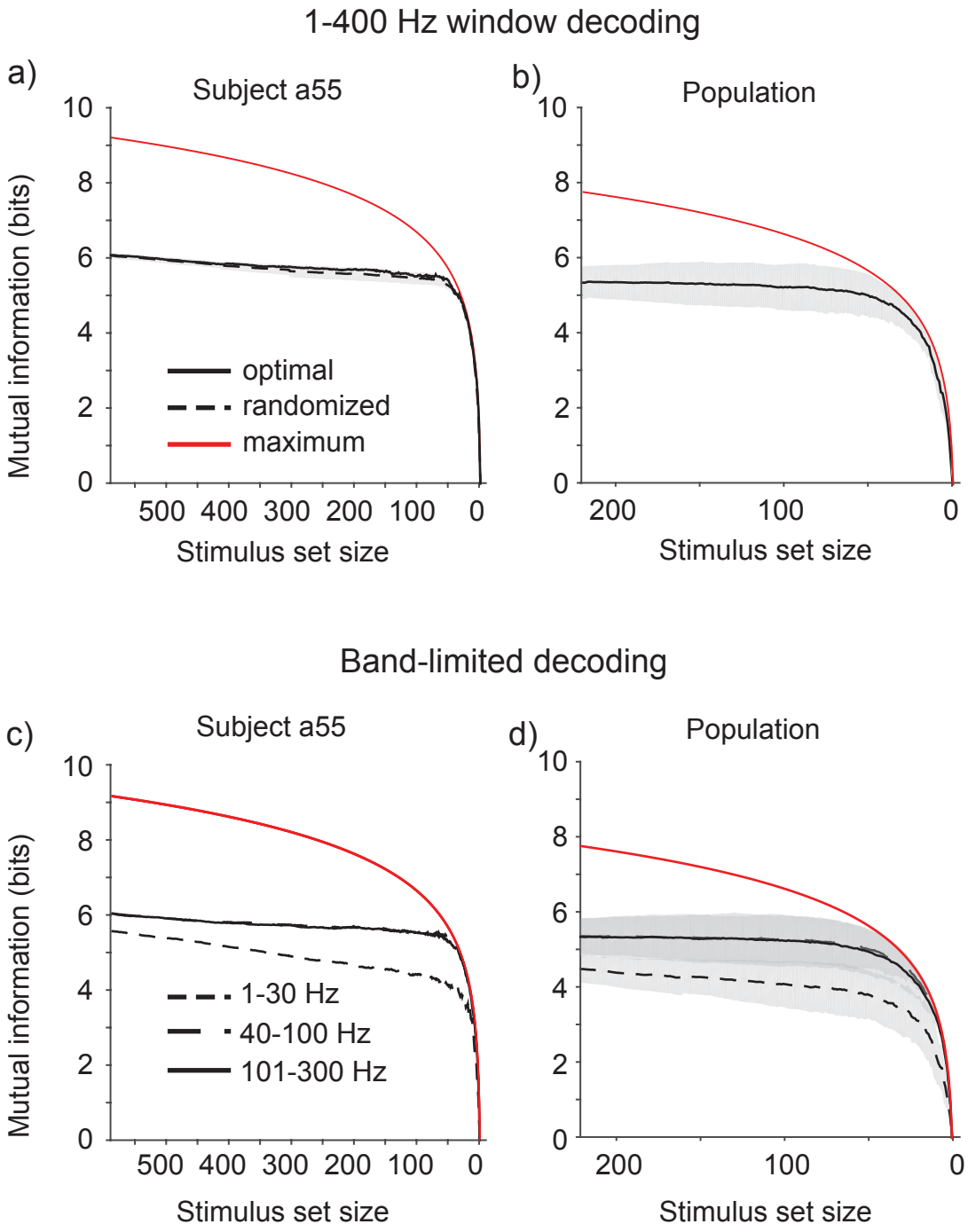
1-400 Hz window decoding
a)
Subject a55
b)
Population
Mutual information (bits)
10
8
6
4
2
0
optimal
randomized
maximum
500 400 300 200 100 0
200 100 0
Stimulus set size
Band-limited decoding
c)
Subject a55
d)
Population
1-30 Hz
40-100 Hz
101-300 Hz